An ICA-EBM-Based sEMG Classifier for Recognizing Lower Limb Movements in Individuals With and Without Knee Pathology

Ganesh R. Naik*, *Senior Member, IEEE*, S. Easter Selvan†, Sridhar P. Arjunan, *Senior Member, IEEE*, Amit Acharyya, *Member, IEEE*, Dinesh K. Kumar, *Senior Member, IEEE*, Arvind Ramanujam, and Hung T. Nguyen, *Senior Member, IEEE*

***Abstract*— Surface electromyography (sEMG) data acquired during lower limb movements has the potential for investigating knee pathology. Nevertheless, a major challenge encountered with sEMG signals generated by lower limb movements is the inter-subject variability, because the signals recorded from the leg or thigh muscles are contingent on the characteristics of a subject such as gait activity and muscle structure. In order to cope with this difficulty, we have designed a three-step classification scheme. First, the multichannel sEMG is decomposed into activities of the underlying sources by means of *independent component analysis* via entropy bound minimization. Next, a set of time-domain features, which would best discriminate various movements, are extracted from the source estimates. Finally, the feature selection is performed with the help of the *Fisher score* and a *scree-plot-based statistical technique*, prior to feeding the dimension-reduced features to the *linear discriminant analysis*. The investigation involves 11 healthy subjects and 11 individuals with knee pathology performing three different lower limb movements, namely, walking, sitting, and standing, which yielded an average classification accuracy of 96.1% and 86.2%, respectively. While the outcome of this study *per se* is very encouraging, with suitable improvement, the clinical application of such an sEMG-based pattern recognition system that distinguishes healthy and knee pathological subjects would be an attractive consequence.**

***Index Terms*— Fisher score, independent component analysis, knee pathology, linear discriminant analysis, surface electromyography.**

I. Introduction

LOWER LIMB motions are inevitable for performing several human activities such as sitting, standing, stair ascent, stair descent, squatting, etc. In order to diagnose neuromuscular and skeletal disorders, the gait analysis is essential that subsumes the classification and assessment of lower limb motions [1]. Since traditional techniques meant for investigating the gait require an extensitive gait laboratory, there is a pressing need to build simpler approaches for the appraisal of gait dysfunction. Several kinematics and non-invasive techniques have been recommended for assessing the lower limb activities. During recent years, the electromyography (EMG)—electrical recordings of muscle activities from the skeletal muscles—has been widely used for this task [1], [2]. These myoelectric signals are extensively sought after for neuropathic and myopathic investigations, prosthetic device control, and rehabilitation [3], [4]. The EMG signals can either be acquired by deploying surface electrodes or with concentric needle electrodes [5]. The former method is mainly followed in prosthetic and rehabilitation applications, whereas the latter in the diagnosis of various neuro-muscular disorders that affect motor units (MUs) [5], [6].

The surface EMG (sEMG) has been a preferred choice for examining the actions and gestures of the upper or lower limb, as well as for prosthetic control [5], [7]. This process includes extracting the features from the sEMG, followed by assigning a signal to one of the various categories of limb movement using a pattern recognition technique [5]. Classifying the sEMG signals corresponding to lower limb movements has been deemed more challenging by researchers than those concerning upper limb movements, because the former signals are complex in nature, and the associated muscles are buried deep beneath the skin with a considerable overlap between each other [8]–[10].

Many studies have been devoted to classify the lower limb sEMG data with various signal processing and pattern recognition methods [11]–[13]. Choi *et al*. applied a *neural network classifier* to recognize the sEMG signal patterns of lower limb muscles during the postural balance recovery of the human body. This study could achieve 75% mean success rate in motion recognition by classifying the sEMG signal into five categories—forward perturbation, backward perturbation, lateral perturbation, and two oblique perturbations [14]. Huang

Asterisk and dagger indicate the corresponding author and co-first author, respectively.

G. R. Naik is with the MARCS Institute, Western Sydney University, Kingswood, NSW–2747, Australia (e-mail: ganesh.naik@westernsydney.edu.au).

S. E. Selvan and A. Ramanujam are with the Human Performance and Engineering Research Lab, Kessler Foundation, West Orange, NJ 07052, U.S.A. (e-mail: ESelvan@kesslerfoundation.org; ARamanujam@kesslerfoundation.org).

S. P. Arjunan and D. K. Kumar are with the Biosignals Lab, RMIT University, Melbourne, VIC 3000, Australia (e-mail: sridhar.arjunan@rmit.edu.au; dinesh@rmit.edu.au).

A. Acharyya is with the Department of Electrical Engineering, Indian Institute of Technology (IIT), Hyderabad 502205, India (e-mail: amit_acharyya@iith.ac.in).

H. T. Nguyen is with the Faculty of Science, Engineering & Technology, Swinburne University of Technology, John Street, Hawthorn VIC 3122, Australia (e-mail: hungnguyen@swin.edu.au).

et al. investigated the sEMG-based pattern recognition methods to identify user locomotion modes and achieved nearly 90% classification accuracy [15]. In another study, Atakan *et al*. proposed an intent recognition approach for the real-time supervisory control of a powered lower limb prosthesis, which could infer the user intent to stand, sit, or walk, by recognizing patterns in prosthesis sensor data [16]. Interestingly, Joshi *et al*. adopted the *Bayesian information criterion* and *linear discriminant analysis* (LDA) to classify different gait phases from the lower limb sEMG of normal subjects [2]. The *fractal analysis* of knee-joint using vibroathrographic (VAG) signals has been reported by Rangayyan *et al*. to observe the change in the *fractal dimension* (FD) for abnormal VAG signals [17]. In a related work, Ryu and Kim identified multiple gait phases using the *support vector machine* (SVM) and LDA to detect the change in the FD pertinent to abnormal VAG signals [18].

Dedicated efforts have been taken in the past to distinguish the patterns in sEMG that characterize the posture and gait of healthy individuals [2], [10], [18]. Of late, there has been a surge of interest in exploring pattern recognition tools that cater to identify the sEMG signals resulting from lower limb movements in subjects having knee issues. Janidarmian *et al.* advocated an automated diagnosis system built around the *bagged decision tree classifier* to classify a set of time-domain features deduced from the sEMG data, which rendered an accuracy of 97.17% in distinguishing healthy subjects from people with knee abnormalities [19]. In spite of its impressive performance, this strategy is limited to only binary classification scenarios. It is noteworthy to briefly discuss the sEMG classification frameworks—*multilayer perceptron artificial neural network* (MP-ANN) in [20], *adaptive local binary pattern* (ALBP) in [21], and *noise-assisted multivariate empirical mode decomposition* (NA-MEMD) in [22]—and to present their outcome, since the classifiers were evaluated with the same dataset that we used for validating our approach. For brevity sake, an account on these schemes has been deferred to Section IV-B.

The activities of daily living (ADLs) are a series of routine activities performed by individuals on a daily basis, and are essential for independent living at home or in the community. The ability to independently sit, stand, and walk is critical towards performing the ADLs. The functionality of the lower limb muscles during each of the task-specific maneuvers—sitting, walking, and standing—is quite different. During standing, the *soleus*, *gastrocnemius*, *tibialis anterior*, *plantarflexors*, and *dorsiflexors* play a key role in maintaining the upright posture. Seated leg extensions involve the recruitment of a powerful group of muscles, namely, the *quadriceps*, whereas a coordinated activation of all lower limb muscles is observed during walking tasks. The diagnosis of knee pathology is therefore facilitated by the direct effects of the disease, which are pronounced in some or all lower limb muscles during some or all of the aforementioned maneuvers. It is thus crucial to perform a task-specific classification of the sEMG patterns, which in turn will enable one to individually study and assess the impact of a knee disorder on a specific lower limb task, i.e., sitting, walking, and standing. The three physical tasks are chosen because these common exercises aid diagnosis, and do not use extra weights with weight-lifting plates, dumbbells, fitness equipment, etc., which would affect the speed and acceleration [20]. Note that since the task of classifying pathological lower limb muscles is a persistent challenge, it certainly deserves further research attention. Furthermore, the sEMG pattern classification has been widely investigated for neural control of external devices in order to assist with movements of patients with motor deficits, because, as of now, limited progress has only been achieved to make EMG-controlled lower limb prostheses commercially available [16]. Hence the objective of this article is to design a robust sEMG classifier, which is capable of distinguishing between the sEMG signals pertaining to lower limb movements in able-bodied subjects and those with knee pathology.

Unlike traditional univariate statistical methods, multivariate techniques can unravel more complex connections between the dependent and independent variables. In that sense, the *independent components analysis* (ICA) is a predominantly applied strategy for source separation or estimation of *independent components* (ICs) subject to the supposition that the observed data stems from linearly mixing these ICs. In view of the sEMG processing, the ICs may closely be related to the *motor unit action potentials* (MUAPs), e.g., ICA for upper limb sEMG applications in [23]–[25]. In general, the ICA algorithms exploit the higher order statistics to minimize the *mutual information* (MI) among the sources. We have adopted a recent approach that estimates sources via entropy bound minimization (ICA-EBM) [26]–[28]. The reason for this choice is that a rigorous simulation study in [29] demonstrates that the ICA-EBM could produce a remarkably accurate set of sources with a meager computational requirement.

A feature vector comprises six time-domain features extracted from the sEMG data, which are believed to be effective in discriminating the movements, as well as the FD estimated from the respective data. The dimension of the feature vector is reduced by an unsupervised statistical method known as the *profile likelihood maximization* (PLM) based on the *Fisher score* (FS), which makes it conducive for the subsequent LDA classifier to accurately predict the lower limb movements responsible for the generation of the sEMG data. The proposed sEMG classifier performance has rigorously been evaluated in the task of identifying the movements—walking, sitting, and standing—associated with knee muscles in healthy individuals and subjects afflicted with knee disorders.

The remainder of the article is organized as follows. Section II provides an in-depth overview of ICA-EBM, FD determination using *Higuchi algorithm*, and PLM. In a broader sense, Section III is devoted to describing the recording and processing of sEMG data as well as the performance evaluation of the classifier. This section covers the details on an exhaustive set of features that in turn is reduced in dimension with the FS-based PLM algorithm and the sEMG data classification by the LDA. In what follows, the quantitative results obtained from the advocated scheme and the related discussion are in order under Section IV-A and IV-B, respectively. Finally, Section V concludes this study with pointers on future perspectives.

II. Technical Preliminaries

A. Source Separation Via Entropy Bound Minimization

Let $\mathbf{z}(t) = [z_1(t), \ldots, z_N(t)]^\top = \mathbf{V}\mathbf{x}(t)$ be the observed signal assumed to have originated from linear mixing of N statistically independent zero-mean sources $\mathbf{x}(t) = [x_1(t), \ldots, x_N(t)]^\top$ through a nonsingular $N \times N$ *mixing matrix* $\mathbf{V}$, where $(\cdot)^\top$ and t represent the matrix transpose operation and time index, respectively. The objective of an ICA algorithm is to recover the *demixing matrix*, $\mathbf{W} = \mathbf{V}^{-1}$, such that the independent source estimates would be yielded via a linear transformation, $\mathbf{y}(t) = [y_1(t), \ldots, y_N(t)]^\top = \mathbf{W}\mathbf{z}(t)$. In practice, this is achieved by minimizing a *contrast function* subject to some constraints. An extensively studied ICA contrast is the MI, expressed as follows in terms of the entropy function $H(\cdot)$

$$I(y_1; \ldots; y_N) = \sum_{n=1}^{N} H(y_n) - \log|\det(\mathbf{W})| - H(\mathbf{z}) \quad (1)$$

where the time index is omitted for simplicity's sake.

Traditional ICA algorithms rely on an entropy estimator to evaluate the MI given in (1). The challenges associated with this category of methods are computational overheads warranted by the nonparametric entropy estimation, sensitivity to outliers in case of *Edgeworth expansion*, and poor performance due to improper assumption on the source densities. Additionally, *a priori* information on the EMG source densities is unavailable in most situations. What we have known so far is that, with respect to a Gaussian distribution, the probability density of EMG is shown to peak more sharply near zero in [30], and the measured EMG density is reported to have a larger kurtosis in [31] and [32]. Nevertheless, on the upside, the ICA-EBM propounded in [28] by Li and Adalı is quite flexible, can approximate the entropies of a wide range of distributions, and hence it remains ideally suited for separating the sources that might have originated from distributions that are sub- or super-Gaussian, unimodal or multimodal, symmetric or skewed by employing only a small class of nonlinear functions [28]. An added merit is the enhancement in the accuracy of source estimates by way of relaxing the orthogonality constraint among the components. A primer that introduces the underlying principle of the ICA-EBM is presented in the ensuing paragraphs. For more technical subtleties related to its implementation, interested readers are directed to [26]–[28].

Let $M(y)$ be a measuring function of a random variable y having zero mean and unit variance; an estimate of its expected value $\widehat{\eta}_M$ can be obtained by averaging the samples of $M(y)$ drawn from the distribution $p(y)$. The crux of the ICA-EBM lies in determining an upper bound for $H(y)$ by solving for the *maximum entropy distribution* (MED) that maximizes the entropy subject to the constraint, $\mathbb{E}[M(y)] = \eta_M$. According to the *principle of maximum entropy*, $p(y)$ maximizes the entropy, $\mathcal{H}[p(y)] = -\int_{-\infty}^{\infty} p(y)\log p(y)dy$, subject to the following set of constraints: $\int_{-\infty}^{\infty} yp(y)dy = 0$; $\int_{-\infty}^{\infty} y^2p(y)dy = 1$; $\int_{-\infty}^{\infty} M(y)p(y)dy = \eta_M$; and $\int_{-\infty}^{\infty} p(y)dy = 1$. The entropy maximization problem is hence formulated as a *Lagrangian function*

$$\begin{aligned}\mathcal{L}[p(y)] = &-\int_{-\infty}^{\infty} p(y)\log p(y)dy + \ell_1\left(\int_{-\infty}^{\infty} p(y)dy - 1\right)\\ &+ \ell_2\int_{-\infty}^{\infty} yp(y)dy + \ell_3\left(\int_{-\infty}^{\infty} y^2p(y)dy - 1\right)\\ &+ \ell_4\left(\int_{-\infty}^{\infty} M(y)p(y)dy - \eta_M\right)\end{aligned}$$

with $\ell_1, \ldots, \ell_4$ being the *Lagrangian multipliers*. It has been shown in [28] that letting $\delta\mathcal{L}[p(y)]/\delta p(y) = 0$ yields

$$p(y) = A\exp[-\alpha y^2 - \beta y - \gamma M(y)]$$

wherein the parameters A, α, β, and γ are determined by taking the constraints into account. The maximum entropy is then expressed as

$$\begin{aligned}\mathcal{H}[p(y)] &= -\int_{-\infty}^{\infty} p(y)\log p(y)dy\\ &= -\log A + \alpha + \gamma\eta_M\\ &= 0.5\log(2\pi e) - \mathcal{N}(\eta_M)\end{aligned}$$

where $0.5\log(2\pi e)$ is the entropy of a standard Gaussian random variable, and $\mathcal{N}(\eta_M) = 0.5\log(2\pi e) + \log A - \alpha - \gamma\eta_M$ is the *negentropy*, which can be numerically solved as explained in the sequel. To this end, one can derive the following functions based on the constraints

$$f_1(\alpha, \beta) = \int_{-\infty}^{\infty} y\exp[-\alpha y^2 - \beta y - \gamma M(y)]d(y) = 0$$

$$f_2(\alpha, \beta) = \int_{-\infty}^{\infty} (1 - y^2)\exp[-\alpha y^2 - \beta y - \gamma M(y)]d(y) = 0.$$

Now α and β values can be deduced with the *Newton iteration*

$$[\alpha_{\text{new}}, \beta_{\text{new}}]^\top = [\alpha, \beta]^\top - \mathbf{J}^{-1}(\alpha, \beta)[f_1(\alpha, \beta), f_2(\alpha, \beta)]^\top$$

for a given $M(y)$ and γ, where $\mathbf{J}(\alpha, \beta)$ denotes the *Jacobian matrix*. Furthermore, by making use of the values of α, β, and γ, the normalization constant A, the expectation η_M, and the negentropy $\mathcal{N}(\eta_M)$ can readily be computed. Thus by evaluating $[\eta_M, \mathcal{N}(\eta_M)]$ at selected points on an interval and interpolating the results, the negentropy value can be returned for any η_M; in other words, the function $\mathcal{N}(\cdot)$ is determined over this interval.

By considering L measuring functions, $M_l(y)$, $l = 1, \ldots, L$, and estimating the expectation $\eta_M^{[l]}$ of each function, an upper bound estimate of $H_l(y)$ given by

$$H_l^{[\text{UB}]}(y) = 0.5\log(2\pi e) - \mathcal{N}(\eta_M^{[l]})$$

can be arrived at. Note that $\mathcal{N}(\eta_M^{[l]})$ is numerically evaluated as described above, and assigned to be zero provided the respective MED does not exist for an estimate of $\eta_M^{[l]}$. The intuitive choice for the estimate of $H(y)$ is the tightest maximum entropy bound defined as

$$\widehat{H}(y) = \min_{1 \le l \le L} H_l^{[\text{UB}]}(y)$$

which in turn is plugged into the expression of MI in (1). The ICA-EBM sequentially updates each row of $\mathbf{W}$ in the

following recast of the problem defined in (1) by dint of a *decoupling method* prescribed in [33]:

$$\mathcal{C}_n(\mathbf{w}_n) = \widehat{H}(y_n) - \log|\mathbf{e}_n^\top \mathbf{w}_n| + K \tag{2}$$

with K and $\mathbf{e}_n$ being a quantity independent of $\mathbf{w}_n$ and a vector of unit length perpendicular to all the rows of $\mathbf{W}$ except $\mathbf{w}_n$, respectively. The decoupling method minimizing the contrast function in (2) deploys a standard vector optimization procedure with a *line-search algorithm* equivalent to that of the FastICA in [34], while still admitting nonorthogonal solutions.

B. Higuchi-Algorithm-Based Fractal Dimension

Higuchi has put forward a strategy in [35] to extract the FD of an irregular time series, which would possibly reflect the complexity and the self-similarity of that signal [36]. Owing to the computation of FD in the time domain, the procedure is acclaimed to be simple and fast [37]. Besides, the Higuchi-algorithm-based FD computation enjoys a stable and reliable outcome [36], [38].

Given a time sequence, $y(1), \ldots, y(T)$, of length T, k time series y_m^k can be constructed as follows:

$$y_m^k = \{y(m), y(m+k), y(m+2k), \ldots, y(m+\lfloor\frac{T-m}{k}\rfloor k)\}$$

where m and k indicate the initial time index and the delay, respectively; $\lfloor\cdot\rfloor$ implies the integer part of the argument. For each time series y_m^k, the average length $L_m(k)$ is defined as

$$L_m(k) := \frac{1}{k}\frac{\sum_{j=1}^{\lfloor\frac{T-m}{k}\rfloor}|y(m+jk)-y(m+(j-1)k)|(T-1)}{\lfloor\frac{T-m}{k}\rfloor k}.$$

Notice that the term $(T-1)/\lfloor(T-m)/k\rfloor k$ serves as a normalization factor. An average length is calculated for all y_m^k's having the same delay k as

$$L(k) = \sum_{m=1}^{k} L_m(k).$$

In practice, the FD denoted as D is estimated by finding the slope of the least square linear fit of the curve—$\ln(L(k))$ versus $\ln(1/k)$—which means that $L(k) \propto k^{-D}$.

C. Profile Likelihood Maximization

Zhu and Ghodsi introduced the PLM algorithm in [39] to estimate the intrinsic dimension of multivariate data from the *scree-plot* of eigenvalues associated with its *principal components*.

Toward this objective, a statistical model is built based on the hypothesis that the given data points denoted as $\mathcal{S} = \{d_1, d_2, \ldots, d_q, \ldots, d_Q\}$ belong to two different *probability distribution functions* (PDFs). The PLM algorithm intends to estimate the index q from the scree-plot of data points such that the set, $\mathcal{S}_1 = \{d_1, \ldots, d_q\}$, and its compliment with respect to $\mathcal{S}$, i.e., $\mathcal{S}_2 = \{d_{q+1}, \ldots, d_Q\}$, are governed by two dissimilar PDFs, $f(\mathbf{d};\boldsymbol{\psi}_1)$ and $f(\mathbf{d};\boldsymbol{\psi}_2)$, respectively. In other words, the algorithm returns the value for q that maximizes the *log-likelihood function*

$$\mathscr{L}(q,\boldsymbol{\psi}_1,\boldsymbol{\psi}_2) = \sum_{i=1}^{q}\log f(d_i;\boldsymbol{\psi}_1) + \sum_{j=q+1}^{Q}\log f(d_j;\boldsymbol{\psi}_2) \tag{3}$$

constructed on the independence assumption. The profile likelihood for a given value of q can thus be obtained by plugging in the *maximum likelihood estimates* (MLEs) of $\boldsymbol{\psi}_1$ and $\boldsymbol{\psi}_2$ deduced from $\mathcal{S}_1$ and $\mathcal{S}_2$, respectively, into (3):

$$\mathscr{L}_q(q) = \sum_{i=1}^{q}\log f(d_i;\widehat{\boldsymbol{\psi}}_1(q)) + \sum_{j=q+1}^{Q}\log f(d_j;\widehat{\boldsymbol{\psi}}_2(q)). \tag{4}$$

For instance, if the PDFs are assumed to be Gaussian, i.e.,

$$f(d;\mu_\kappa,\sigma^2) = \frac{1}{\sqrt{2\pi\sigma^2}}\exp\left[-\frac{(d-\mu_\kappa)^2}{2\sigma^2}\right], \quad \kappa = 1,2$$

the MLEs are given by

$$\widehat{\mu}_1 = \frac{\sum_{d_i\in\mathcal{S}_1} d_i}{q}$$
$$\widehat{\mu}_2 = \frac{\sum_{d_j\in\mathcal{S}_2} d_j}{Q-q}$$
$$\widehat{\sigma}^2 = \frac{(q-1)\widehat{\sigma}_1^2 + (Q-q-1)\widehat{\sigma}_2^2}{Q-2}$$

where

$$\widehat{\sigma}_1^2 = \frac{\sum_{d_i\in\mathcal{S}_1}(d_i-\widehat{\mu}_1)^2}{q}$$
$$\widehat{\sigma}_2^2 = \frac{\sum_{d_j\in\mathcal{S}_2}(d_j-\widehat{\mu}_2)^2}{Q-q}.$$

Note that in (4), the MLEs of $\boldsymbol{\psi}_1$ and $\boldsymbol{\psi}_2$ are denoted as functions of q, since these estimates are contingent on q. As alluded to in [39], an exhaustive search is resorted to for the evaluation of $\mathscr{L}_q(\iota)$, $\iota = 1, \ldots, Q$, and the value of ι for which (4) attains the maximum, as given by

$$\widehat{q} := \arg\max_{\iota=1,\ldots,Q}\mathscr{L}_q(\iota)$$

is deemed as the estimate of q.

III. Methodology

In the proposed method, the sEMG signals recorded with the surface electrodes from four knee muscles are first preprocessed, and then supplied to the ICA-EBM algorithm described in Section II-A to extract the underlying sources. Next, a set of time-domain features and the FDs of the source estimates are computed. An optimal subset of feature components derived from the training dataset that yield a significantly large FS is selected subsequently via the PLM algorithm presented in Section II-C. Finally the LDA algorithm is employed in order to classify the sEMG signals pertaining to the test dataset into three classes of lower limb movements, i.e., sitting, standing, and walking. The schematic diagram of the lower limb movement recognition system is shown in Fig. 1.

A. Data Acquisition

We have tested our sEMG classifier framework with the sEMG data available at the UC Irvine Machine Learning Repository [40], which were acquired from 22 male participants older than 18 years of age. The subjects include 11 healthy ones without any knee injury or pain and 11

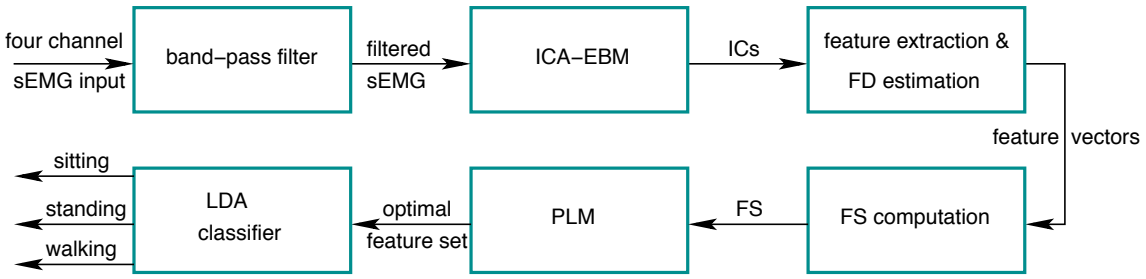

Fig. 1. Schematic diagram of the ICA-EBM-based sEMG classifier for lower limb movement recognition.

individuals with knee pathology—six with anterior cruciate ligament (ACL) injury, four having meniscus injury, and one suffering from sciatic nerve injury. The data collection was carried out by means of an EMG instrument (DataLog MWX8 by Biometrics Ltd.) and a goniometer, while the subjects were undergoing three movements in order to investigate the behavior of knee muscles in the course of gait, leg extension from a sitting position, and flexion of the leg up. Four surface electrodes were spaced apart by 20 mm with a high input impedance (>10 $\mathrm{M}\Omega$) that would obviate the need for a conductive gel. These sEMG electrodes were placed on the surface of the muscles, namely, *vastus medialis* (vm), *semitendinosus* (st), *biceps femoris* (bf), and *rectus femoris* (rf), along the muscle fiber orientation, whereas the goniometer was attached to the external side of the knee joint. For the placement of four sEMG electrodes, the affected limb and the left leg were chosen for the patient population and able-bodied subjects, respectively. The recorded signals from all the four sensors were taken into account for the sitting, standing, and walking task. The data acquisition during the three lower limb movements was not randomized. The gait data pertains to an "over-ground walk", wherein the participants were required to walk on level ground and in a straight path. In addition, the subjects were free to select their own speed during walking, which could induce variations. Despite the possibility to monitor walking-speed-related variations by a goniometer, they are not necessarily to be accounted for in our study, since we consider merely the sEMG data for classifying the movements (without relying on the information from the goniometer). The sEMG signals were stored directly in the internal storage of MWX8-Biometrics with a microSD card and transmitted in real-time through a bluetooth adapter with a resolution of 14 bits and a sampling frequency of 1000 Hz. In addition, the signals were band-pass filtered using a fourth-order Butterworth FIR filter with a frequency range between 20 and 460 Hz.

Recall that the sEMG dataset available in an online repository (refer to [40]) has been used for the experiments. There was neither any synchronism during a movement execution, nor was the time normalization carried out for the dataset prior to data analyses. Moreover, the dataset does not include the sEMG signals corresponding to transition states, i.e., standing to walking, standing to sitting, etc.

B. Data Processing

The band-pass filtered sEMG data was supplied to the ICA-EBM algorithm to extract the source estimates, which in turn were divided into data segments, each one comprising 256 samples, with an overlap of 64 samples between adjacent segments. To facilitate the sEMG classification, the following set of time-domain features was derived from an sEMG data segment, which can be regarded as a time series $y(t)$, $t = 1, \ldots, T$. Furthermore, the FD was estimated from each data segment in a manner described in Section II-B.

1) Extracted Features:

- **Auto Regressive (AR) Model**. For a time series, which is stochastic and sufficiently stationary, the AR model of order p is written as

$$y(t) = -\sum_{i=1}^{p} a_i y(t-i) + e(t)$$

  with a_i and $e(t)$ being the AR parameters and white noise, respectively.
- **Mean Absolute Value (MAV)**. It is calculated by taking the average of the absolute value of a time series as shown below

$$\mathrm{MAV} := \frac{1}{T}\sum_{t=1}^{T} |y(t)|.$$

- **Variance (VAR)**. For a zero-mean time series, the variance—mean value of the square of the deviation of each time sample—can be simplified as

$$\mathrm{VAR} := \frac{1}{T-1}\sum_{t=1}^{T} y(t)^2.$$

- **Root Mean Square (RMS)**. It is expressed as the square root of the arithmetic mean of the squared sample amplitude of a time series as follows

$$\mathrm{RMS} := \sqrt{\frac{1}{T}\sum_{t=1}^{T} y(t)^2}.$$

- **Waveform Length (WL)**. For a given a time series, the cumulative change in amplitude between adjacent samples is computed as

$$\mathrm{WL} := \sum_{t=2}^{T} |y(t) - y(t-1)|.$$

- **Zero Crossings (ZC)**. The total occurrences of sign change—switching from a positive to a negative amplitude and vice versa—in a time series is given by

$$\mathrm{ZC} := \sum_{t=2}^{T} \zeta(t),$$

where

$$\zeta(t) = \begin{cases} 1, & \text{if} \quad \mathrm{sgn}(-y(t) \times y(t-1)) \quad \text{and} \\ & \quad |y(t) - y(t-1)| \geq \epsilon \\ 0, & \text{otherwise} \end{cases}$$

with sgn and ϵ being the signum function and the user-defined threshold, respectively.

We have chosen these time-domain features based on the fact that the RMS, fourth-order AR, and WL are reported to have improved the sEMG classification accuracy involving upper and lower limb movements compared to well-known frequency-domain methods such as the *Fourier transform* and *wavelet transform*. Besides, it has been claimed that the RMS and AR coefficients are computationally efficient and insensitive to electrode displacements [41].

2) Feature Dimensionality Reduction: In the sequel, each feature is denoted by a vector of length 28

$$\begin{aligned} \mathbf{f}_i = [&\mathrm{AR}_{\mathrm{vm}}, \mathrm{AR}_{\mathrm{st}}, \mathrm{AR}_{\mathrm{bf}}, \mathrm{AR}_{\mathrm{rf}}, \mathrm{RMS}_{\mathrm{vm}}, \ldots, \mathrm{RMS}_{\mathrm{rf}}, \\ &\mathrm{MAV}_{\mathrm{vm}}, \ldots, \mathrm{MAV}_{\mathrm{rf}}, \mathrm{VAR}_{\mathrm{vm}}, \ldots, \mathrm{VAR}_{\mathrm{rf}}, \mathrm{WL}_{\mathrm{vm}}, \ldots, \\ &\mathrm{WL}_{\mathrm{rf}}, \mathrm{ZC}_{\mathrm{vm}}, \ldots, \mathrm{ZC}_{\mathrm{rf}}, \mathrm{FD}_{\mathrm{vm}}, \ldots, \mathrm{FD}_{\mathrm{rf}}]^\top \end{aligned}$$

where $i = 1, \ldots, N_{\mathrm{train}}$ with N_{train} being the total number of data segments in the training dataset. The subscript of a feature vector component indicates the muscle from where the sEMG has been recorded. Therefore, the entire set of features can be represented as a matrix $\mathbf{F} \in \mathbb{R}^{28 \times N_{\mathrm{train}}} = [\mathbf{f}_1, \ldots, \mathbf{f}_{N_{\mathrm{train}}}]$. This allows us to denote each row of $\mathbf{F}$ as a vector of length N_{train}, e.g., the second row of $\mathbf{F}$ is given by $\mathbf{f}^2 = [\mathrm{AR}_{\mathrm{st}}^{(1)}, \ldots, \mathrm{AR}_{\mathrm{st}}^{(N_{\mathrm{train}})}]$, where the superscript within the parentheses stands for the index of the data segment. The feature dimensionality reduction attempts to find a subset of feature components such that in the space spanned by the dimension-reduced features, the between-class distances remain as large as possible while the within-class distances are kept as small as possible. Since it requires to solve a combinatorial optimization problem, an expedient strategy is to alleviate the complexity by relying on the FS, wherein a score is computed for each feature component separately according to a criterion $\mathcal{F}$ in (5). Let μ_k^j and σ_k^j denote the mean and standard deviation (SD) of the elements in the j-th row of $\mathbf{F}$ that belong to the k-th class, respectively, and let μ^j represent the mean of all the elements that constitute the j-th row. Then FS can be defined as

$$\mathcal{F}(\mathbf{f}^j) = \frac{\sum_{k=1}^{C} (\mu_k^j - \mu^j)^2}{\sum_{k=1}^{C} (\sigma_k^j)^2}. \tag{5}$$

After computing the FS for each feature component, a heuristics would pick the top-q ranked feature components with large scores. In lieu of deciding q by naive methods, we employ the PLM described in Section II-C, which is premised on statistical reasoning. The FS values of the feature components supplied to the PLM are plotted in the descending order to form a scree-plot, whose "elbow" point corresponds to the value of q. Thus, in the present setting, the PLM has been tailored to select a set of (sub)optimal feature components, which would reduce the computational overheads of the ensuing classification task, and hopefully preserve the accuracy of the sEMG classifier.

3) Feature Classification: Admittedly, options abound for the sEMG classification in general, e.g., SVM, neural network, and *k-nearest neighbor algorithm*; however, the LDA has been proven effective in the context of lower limb sEMG [25], [42], [43]. In principle, the discriminant ability of LDA is enhanced during classification by maximizing the ratio of the between-class variance to the within-class variance. Consider $\mathbf{f}_i^k$ as the i-th feature vector that belongs to class k of cardinality N_k; now by denoting the sample mean of the feature vectors bearing class label k and the overall sample mean as $\boldsymbol{\mu}_k$ and $\boldsymbol{\mu}$, respectively, the within-class scatter matrix $\mathbf{S}_{\mathrm{w}}$ and between-class scatter matrix $\mathbf{S}_{\mathrm{b}}$ can formally be defined as

$$\mathbf{S}_{\mathrm{w}} := \sum_{k=1}^{C} \sum_{i=1}^{N_k} (\mathbf{f}_i^k - \boldsymbol{\mu}_k)(\mathbf{f}_i^k - \boldsymbol{\mu}_k)^\top \tag{6}$$

$$\mathbf{S}_{\mathrm{b}} := \sum_{k=1}^{C} (\boldsymbol{\mu}_k - \boldsymbol{\mu})(\boldsymbol{\mu}_k - \boldsymbol{\mu})^\top. \tag{7}$$

The LDA classifier is endowed with the following merits: (1) It does not require iterative training; (2) It precludes the chances of under- or over-training of data, thereby resulting in high classification accuracies [42]; and (3) With a good linear approximation of a high-dimensional space via feature reduction, it remains as a simple yet an efficient mechanism.

C. k-fold cross validation

In view of improving the reliability of classification results by simple *holdout method*, a *k-fold cross validation strategy* is resorted to for evaluating the sEMG classifier performance, where k is three. This requires the dataset to be randomly partitioned into k subsets, and the holdout method to be repeated k times (folds). Each time, one of the k subsets is treated as a test dataset, whereas the rest of the $k-1$ subsets jointly form a training dataset. The mean classification accuracy across all k trials has been reported, thereby removing the dependency on how the data is divided. The cardinality of the feature set being classified is roughly in the order of 50000, for instance, if 13 features are recommended by the PLM approach, the dataset will have 51580 elements (60 segments$\times$22 subjects$\times$13 features$\times$3 tasks). Specifically in our case, the training and test datasets comprise randomly selected 70% and 30% elements, respectively, in each trial, that jointly constitute the original feature set. Care has been taken to ensure that every data point is included in the test dataset exactly once, and is an element of a training dataset $k-1$ times. Note that the training dataset has exclusively been used for the feature dimensionality reduction task described in Section III-B.2 and for optimizing the LDA model parameters.

D. Performance Evaluation Metrics

Apropos of quantifying the correct classification of normal and pathological samples by our approach, the following statistical metrics have been adopted: (1) sensitivity (Se); (2) specificity (Sp); and (3) accuracy (Ac). By denoting the true positive, true negative, false positive, and false negative outcome of the sEMG classifier as P_{T}, N_{T}, P_{F}, and N_{F}, respectively, the aforementioned metrics are given by

$$\mathrm{Se} := \frac{P_{\mathrm{T}}}{P_{\mathrm{T}} + N_{\mathrm{F}}} \times 100\% \tag{8}$$

$$\mathrm{Sp} := \frac{N_{\mathrm{T}}}{N_{\mathrm{T}} + P_{\mathrm{F}}} \times 100\% \tag{9}$$

$$\mathrm{Ac} := \frac{P_{\mathrm{T}} + N_{\mathrm{T}}}{P_{\mathrm{T}} + N_{\mathrm{T}} + P_{\mathrm{F}} + N_{\mathrm{F}}} \times 100\%. \tag{10}$$

Additionally, we have provided the *confusion matrix* also known as the *error matrix* for the visualization of our classifier performance. In other words, it enables one to easily scrutinize whether the algorithm mislabels the data that belongs to one class as another. While each column of the matrix $\mathbf{C}$ represents the percentage of instances in a predicted class, each row indicates the instances in percentage in an actual class or vice versa. Specifically the outcome of this study can be summarized using the matrix

$$\mathbf{C} = \begin{bmatrix} C_{\mathrm{WW}} & C_{\mathrm{WS}} & C_{\mathrm{WT}} \\ C_{\mathrm{SW}} & C_{\mathrm{SS}} & C_{\mathrm{ST}} \\ C_{\mathrm{TW}} & C_{\mathrm{TS}} & C_{\mathrm{TT}} \end{bmatrix}$$

where the subscripts W, S, and T imply the walking, sitting, and standing, respectively. For instance, C_{WS} is calculated as follows:

$$C_{\mathrm{WS}} = \frac{\text{No. of cases in class W predicted as class S}}{\text{Total cases predicted as class S}} \times 100\%.$$

Since all the correct predictions are located along the main diagonal of the matrix, the errors can easily be noticed by visually inspecting the off-diagonal elements.

IV. Results and Discussion

A. sEMG Classification Results

To begin with, the feature components were listed along the abscissa of Fig. 2 in the decreasing order of their FS, which in turn were computed from a training dataset. Next, a scree-plot was constructed by linking the points that represent the FS values shown in the ordinate. Upon feeding the FS values to the PLM algorithm detailed in Section II-C, the stochastic method determined the supposedly elbow point (orange vertical line segment) of the scree-plot. A subset of the feature components located to the left of the elbow point is deemed relevant to the lower limb movement recognition task. Phrased differently, this subset gave rise to the dimension-reduced features, with which the movement pertinent to an sEMG signal belonging to a test dataset was identified by the LDA algorithm. The sEMG classifier performance has been quantified in percentage of metrics defined in (8) to (10) and consolidated in Table I, which reflect how reliably the lower limb movement could be predicted by analyzing the signals recorded during the task. Essentially, we studied the percentage of accuracy with which the sEMG classifier could reveal whether a recorded sEMG signal pertains to either walking or sitting or standing. Table II reports the subject-wise mean and SD of the correct classification percentage for the sEMG data acquired from healthy individuals, whereas the results concerning the subjects with knee pathology are compiled in Table III. The percentage of success (mean and SD) attained by the classifier while assigning the sEMG data from normal subjects into three known classes—walking, sitting, and standing—is concisely given by the mean confusion matrix in Table IV. Similarly, the exact classification in percentage (mean and SD) for the subjects suffering from knee pathology is displayed in Table V. In Table IV and V, the diagonal elements indicate the classification accuracy in percentage in the case of subjects without and with knee pathology, respectively.

We have also performed an investigation to assess the influence of source separation on the sEMG classifier performance. To this end, the classification pipeline outlined in Section III was modified by precluding the ICA module. This means that the reduced set of features extracted directly from the filtered and segmented sEMG signals was supplied to the LDA classifier. Since the blind source separation such as the ICA is meant to separate the sources from their mixtures subject to the (statistical) independence constraint, one may anticipate that the classifier performance would remarkably improve when the features are derived from the intrinsic sources identified by the ICA-EBM approach rather than from the actual sEMG recordings. We learn that the computational efforts due to the implementation of ICA-EBM have indeed paid off in the proposed scheme as the classification outcome listed in Table II and III corroborates with this claim. To summarize, the source separation entailed an increase in the average classification accuracy across all subjects and lower limb movements from 74.7% to 96.1% and 65.9% to 86.2% for the healthy population and individuals with knee ailments, respectively.

B. Discussion

As noted in Section I, we summarize and compare the contributions akin to ours—in the sense that these schemes made use of the dataset with which we validated our approach. Herrera-González *et al*. segregated a combination of sEMG and goniometric signals into three classes defined by the lower limb movement [20]. Toward this goal, the time-frequency and wavelet transform features were derived from the data and classified using an MP-ANN with an accuracy of 88%, 92%, and 94% for walking, sitting, and standing task, respectively. The performance metrics estimated from this experiment are listed in Table VI. Despite good classification accuracy for the pooled data (combination of normal subjects and knee patients), the classifier performance for the individual population remains intractable. Moreover, this study relies on two modalities—sEMG and goniometer—to achieve this end. Ertuğrul *et al*. developed an ALBP for extracting features based on local changes in an sEMG signal, and demonstrated its ability to discriminate between the healthy and knee pathological

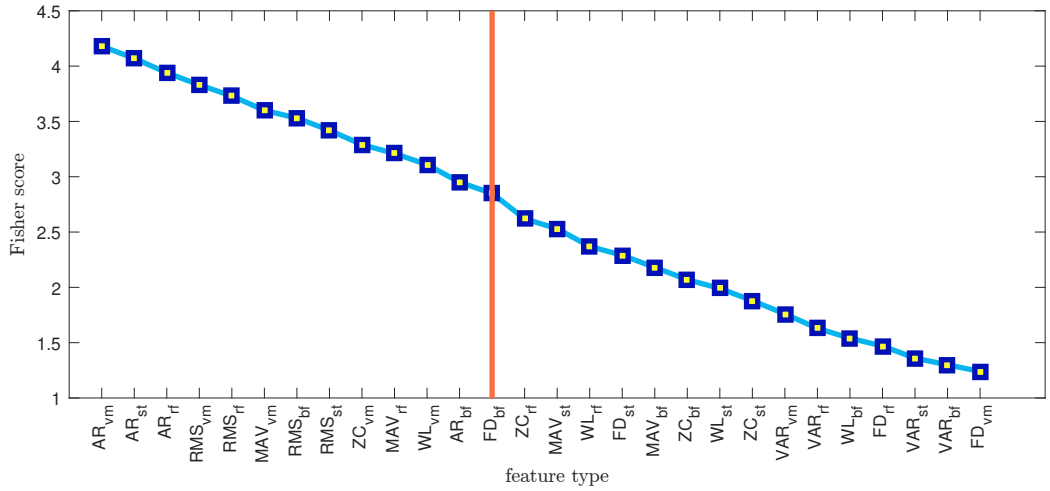

Fig. 2. The scree-plot (light blue curve) is constructed using the FS (dark blue squares filled with yellow) computed for the 28 feature components—six time-domain features and the FD from four knee muscles. The PLM algorithm determines the elbow point (orange vertical line segment) associated with the index of FD_{bf} in a k-fold cross validation trial. Consequently, the reduced feature subset $[AR_{vm}, AR_{st}, AR_{rf}, RMS_{vm}, RMS_{rf}, MAV_{vm}, RMS_{bf}, RMS_{st}, ZC_{vm}, MAV_{rf}, WL_{vm}, AR_{bf}, FD_{bf}]^T$ is only considered by the subsequent LDA classifier stage for further analysis.

TABLE I

OVERALL MEAN AND SD OF LDA CLASSIFIER PERFORMANCE METRICS IN PERCENTAGE FOR A HEALTHY POPULATION AND SUBJECTS HAVING KNEE PATHOLOGY, WHILE SEMG WAS COLLECTED DURING THREE LIMB MOVEMENTS—WALKING, SITTING, AND STANDING.

Performance metric	Healthy subjects			Subjects with knee pathology		
	Walking	Sitting	Standing	Walking	Sitting	Standing
Se	95.1 ± 1.3	95.4 ± 1.2	95.3 ± 1.3	84.6 ± 1.3	84.8 ± 1.3	83.1 ± 1.2
Sp	98.2 ± 1.2	98.6 ± 1.1	98.6 ± 1.2	89.2 ± 1.2	89.0 ± 1.2	88.4 ± 1.3
Ac	96.0 ± 1.3	96.2 ± 1.2	96.2 ± 1.3	86.6 ± 1.3	86.4 ± 1.3	85.5 ± 1.3

TABLE II

SUBJECT-WISE MEAN AND SD OF CORRECT SEMG CLASSIFICATION IN PERCENTAGE FOR HEALTHY INDIVIDUALS UNDER THE FOLLOWING CONDITIONS: GAIT (WALKING), LEG EXTENSION FROM A SITTING POSITION, AND FLEXION OF THE LEG UP (STANDING).

Subject	Source separation precluded			ICA-EBM included		
	Walking	Sitting	Standing	Walking	Sitting	Standing
1	73.4 ± 1.1	75.3 ± 1.2	75.3 ± 1.2	95.6 ± 1.2	96.2 ± 1.3	96.3 ± 1.3
2	72.2 ± 1.2	75.1 ± 1.3	75.2 ± 1.3	96.3 ± 1.3	96.4 ± 1.2	96.4 ± 1.3
3	73.8 ± 1.3	74.9 ± 1.3	75.6 ± 1.2	95.8 ± 1.4	96.1 ± 1.2	96.2 ± 1.2
4	73.1 ± 1.1	75.3 ± 1.2	74.2 ± 1.3	96.4 ± 1.3	96.3 ± 1.1	96.3 ± 1.3
5	73.4 ± 1.2	74.2 ± 1.4	75.4 ± 1.2	96.1 ± 1.4	96.2 ± 1.0	95.6 ± 1.1
6	73.6 ± 1.3	75.4 ± 1.2	75.3 ± 1.3	95.6 ± 1.6	96.3 ± 1.4	96.1 ± 1.4
7	73.2 ± 1.2	75.3 ± 1.1	75.8 ± 1.2	96.2 ± 1.1	96.1 ± 1.1	95.8 ± 1.2
8	73.4 ± 1.1	75.6 ± 1.2	75.9 ± 1.3	96.3 ± 1.5	96.2 ± 1.4	96.2 ± 1.3
9	74.2 ± 1.3	75.2 ± 1.3	75.6 ± 1.2	95.8 ± 1.3	96.1 ± 1.2	96.4 ± 1.3
10	73.8 ± 1.4	75.3 ± 1.2	75.3 ± 1.3	95.9 ± 1.4	96.3 ± 1.2	96.5 ± 1.2
11	73.6 ± 1.3	76.1 ± 1.4	75.8 ± 1.4	95.8 ± 1.2	96.3 ± 1.3	96.2 ± 1.5

subjects with an accuracy of 85% [21]. Recently, Zhang *et al*. attempted a lower-limb-movement-based classification of the sEMG data from able-bodied subjects by means of an NA-MEMD [22]. The outcome of this study is presented in Table VII. Note that the sEMG classifier described in [21] is only meant for making a binary decision, and the one propounded in [22] reports results restricted to the healthy group.

In the present work, the type and the total number of components in the dimension-reduced feature set may vary across the 3-fold cross validation trials, since the PLM uses different training datasets that are randomly selected prior to classification. The FD of an sEMG signal is thought to possess valuable information on the complex nature of the signal and the randomness associated with physiological conditions. Therefore, we chose to add the FD along with the time-domain feature set, which would hopefully retain the signal properties crucial for discriminating the movements. Note, however, that

TABLE III

SUBJECT-WISE MEAN AND SD OF SEMG CLASSIFIER ACCURACY IN PERCENTAGE FOR INDIVIDUALS SUFFERING FROM KNEE PATHOLOGY. THE SEMG WAS ACQUIRED DURING THE EXPERIMENTAL CONDITIONS, NAMELY, WALKING, SITTING, AND STANDING.

Subject	Source separation precluded			ICA-EBM included		
	Walking	Sitting	Standing	Walking	Sitting	Standing
1	65.3 ± 1.2	65.3 ± 1.2	66.3 ± 1.2	87.7 ± 1.3	86.4 ± 1.4	85.8 ± 1.3
2	65.4 ± 1.3	66.4 ± 1.1	66.3 ± 1.3	86.8 ± 1.2	86.5 ± 1.2	85.2 ± 1.2
3	65.3 ± 1.1	65.6 ± 1.2	66.4 ± 1.2	86.4 ± 1.3	86.7 ± 1.3	85.4 ± 1.3
4	65.2 ± 1.4	66.2 ± 1.3	66.2 ± 1.3	86.4 ± 1.4	86.4 ± 1.2	85.5 ± 1.2
5	65.2 ± 1.2	66.4 ± 1.2	66.4 ± 1.4	86.8 ± 1.2	86.5 ± 1.6	85.4 ± 1.4
6	65.5 ± 1.0	66.2 ± 1.4	66.2 ± 1.2	86.3 ± 1.3	86.4 ± 1.4	85.5 ± 1.1
7	65.6 ± 1.2	66.4 ± 1.2	66.3 ± 1.4	86.4 ± 1.4	86.3 ± 1.3	85.7 ± 1.5
8	65.6 ± 1.3	66.2 ± 1.2	66.4 ± 1.3	86.3 ± 1.3	86.8 ± 1.2	85.4 ± 1.2
9	65.2 ± 1.2	66.4 ± 1.3	66.5 ± 1.2	86.7 ± 1.2	86.3 ± 1.3	85.5 ± 1.4
10	65.6 ± 1.4	66.5 ± 1.4	66.3 ± 1.3	86.8 ± 1.5	86.2 ± 1.4	85.8 ± 1.3
11	65.4 ± 1.2	65.9 ± 1.2	66.2 ± 1.2	86.4 ± 1.2	86.3 ± 1.2	85.5 ± 1.4

TABLE IV

MEAN CONFUSION MATRIX FOR LDA CLASSIFICATION RESULTS IN PERCENTAGE FOR HEALTHY INDIVIDUALS. BOLDFACED DIAGONAL ELEMENTS INDICATE THE CLASSIFICATION ACCURACY.

Class	Classified as					
	Walking		Sitting		Standing	
	μ	σ	μ	σ	μ	σ
Walking	**96.0**	1.3	2.4	0	1.5	0
Sitting	1.7	0	**96.2**	1.2	1.3	0
Standing	2.3	0	1.4	0	**96.2**	1.3

TABLE V

MEAN CONFUSION MATRIX FOR LDA CLASSIFIER OUTCOME IN PERCENTAGE FOR INDIVIDUALS WITH KNEE DISORDER. THE CLASSIFICATION ACCURACY IS DENOTED IN BOLDFACE.

Class	Classified as					
	Walking		Sitting		Standing	
	μ	σ	μ	σ	μ	σ
Walking	**86.6**	1.3	7.8	0	8.6	0
Sitting	7.5	0	**86.4**	1.3	5.9	0
Standing	5.7	0	5.8	0	**85.5**	1.3

TABLE VI

OVERALL MEAN AND SD OF MP-ANN CLASSIFIER PERFORMANCE METRICS IN PERCENTAGE REPORTED IN [20], WHILE THE SEMG DATA DURING THREE LIMB MOVEMENTS—WALKING, SITTING, AND STANDING—WERE POOLED FROM ABLE-BODIED AND KNEE PATHOLOGICAL SUBJECTS. NOTE THAT THE DATASET IS THE ONE THAT WAS TESTED IN OUR STUDY.

Performance metric	Able-bodied and knee pathological subjects		
	Walking	Sitting	Standing
Se	87	93	87
Sp	92	96	100
Ac	88	94	92

the FD remains incapable of differentiating the tasks that have subtle changes among themselves, even though it lends itself to study the signal properties apposite to pathological conditions [44]. Furthermore, the dimensionality based on fractal analysis is known to be highly sensitive for hidden rhythms on sEMG in subjects under fatigue, pathology, and the condition of increased MU synchronization [45], [46]. This could be the rationale behind why the FD component has often been disregarded by the PLM.

In able-bodied subjects, the performance metrics, namely, Se, Sp, and Ac, of the sEMG classifier are found to be somewhat consistent, irrespective of the lower limb movements. Nevertheless, there is a decline in the values of these metrics, when the classifier is deployed to recognize the tasks carried out with a knee disorder. Observe that the performance degradation is noticeable with pathological cases engaged in a standing task. Provided the correct class label is either sitting or standing, the misclassified data have almost been distributed similarly among the other two groups in Table IV and V. Whereas, in healthy and pathological subjects, the misclassifications corresponding to walking fall into the remaining two categories in disparate proportions, suggesting possible changes induced by knee pathology in the physiology of walking.

Several muscles are involved in the biomechanics of the knee, which facilitate the realization of disparate movements. The mundane tasks such as sitting, walking, and standing that deploy leg muscles cause enhanced levels of quadriceps and hamstring muscle activities [47]. Such movements are more likely to be altered, provided the individual is suffering from knee-related ailments, e.g., ACL, meniscus injury, and sciatic nerve injury, which may cause dysfunction of the knee-joint and significantly disrupt the normal course of life [20]. Currently, the gait-analysis-based diagnosis is on the rise for treating knee ailments. However, serious setbacks are that it requires an extensive infrastructure such as a purpose-built gait laboratory, the usage of which is expensive and restricted to large urban hospitals, thereby inducing delays while patients seek assessment. Hence, from the viewpoint of an aging

TABLE VII
MEAN AND SD OF EMD, MEMD, AND NA-MEMD CLASSIFICATION RESULTS REPORTED IN [22], WHEN APPLIED TO THE SEMG DATASET USED IN OUR EXPERIMENTS.

Walking			Sitting			Standing		
EMD	MEMD	NA-MEMD	EMD	MEMD	NA-MEMD	EMD	MEMD	NA-MEMD
0.64 ± 0.14	0.73 ± 0.10	0.79 ± 0.03	0.67 ± 0.11	0.79 ± 0.07	0.83 ± 0.05	0.69 ± 0.06	0.82 ± 0.06	0.83 ± 0.06

population, there is a dire need for diagnostic tools that are economically viable and suitable for a general-purpose clinic.

Previous research findings have established the fact that the sEMG signals collected from the hamstring and quadriceps muscles are indeed instrumental for investigating the movement disorders of the knee [19]–[21]. In this respect, the sEMG is arguably one of the preferred electrophysiological modalities, because it is non-invasive, inexpensive, and can be recorded wirelessly. Nonetheless, as can be inferred from earlier studies, it suffers from poor accuracy as a result of *cross-talk* due to overlapping muscles. Therefore, there is a growing need to further refine the sEMG processing pipeline to analyze and label the recordings in terms of knee movements, which would enable the clinicians to keep track of the alterations caused by knee pathology.

One must bear in mind that the gait sEMG signals are generally known to have a large variation while performing a single task, thereby resulting in overlapping of features among different tasks. This in turn would affect the outcome of an algorithm devoted to classification tasks. Most importantly, the performance of the proposed lower limb sEMG classifier degrades noticeably as it is supplied with the sEMG signals from the leg muscles of subjects with knee pathology. This is indeed a foreseen difficulty, and any classifier algorithm would face challenges owing to the following rationale.

Following a knee injury, particularly in the case of ACL, a ligament reconstruction is performed with the harvested hamstring muscle tendon. As a consequence, the hamstring muscle volume in the reconstructed limb remains significantly smaller than that of a normal limb [48]. A downside of atrophy and shortening of hamstring muscles is that they could adversely interfere with the rehabilitation that requires high levels of muscle activation. We therefore speculate that the combined effect of reduced hamstring muscle activity as well as the interaction of the muscle length and the anatomical location of the tendons would contribute to variations in the acquired sEMG data during a lower limb movement, thereby affecting the sEMG classification accuracy.

Many studies have reported an appreciable gender difference in muscle activities, for instance, the knee extensor muscles as well as the contact and pressure area of the *patellofemoral joint* are endowed with more strength in men [49], [50]. However, the undesirable effect due to this difference could be deterred by including only the subjects from the same gender. It still remains unclear how to select appropriate muscles such that the classification inaccuracies caused by the hamstring muscles of an individual with injured knees do not significantly impair the overall classifier performance.

Even though the extracted features exhibit some differences across various knee disorders, it remains difficult to ascertain this statistically due to a small sample size under each category. We speculate that the composition of various conditions (six with ACL, four having meniscus injury, and one with sciatic nerve injury) to form a heterogeneous knee pathological dataset would indeed have a negative impact on the classification results. However, owing to the limitations imposed by a small sample size, we could not validate this effect. These are interesting pointers for future research, which necessitate a larger dataset with sufficient candidates under each type of knee pathology. In a nutshell, the results reported by the sEMG classifier are therefore independent of the prior knowledge that we have concerning the type of disorder.

V. CONCLUSION

An ICA-based classification scheme for lower limb sEMG data has been designed and tested with signals recorded from healthy individuals as well as subjects suffering from knee pathology. The ICA-EBM technique was adopted to decompose the band-pass filtered sEMG data into its constituent MUAPs. A reduced set of time-domain features and FDs, as recommended by a dimensionality reduction scheme, was extracted from the source estimates. Finally, the sEMG data was assigned to any one of the three categories—walking, sitting, and standing—with the aid of the LDA algorithm supplied with the feature subset.

Traditional analyses of sEMG signals from knee-support muscles are known to suffer from poor accuracy in differentiating three major tasks, i.e., walking, sitting, and standing. On that account, this study focuses on improving the sEMG classification accuracy by incorporating a source separation module into the lower limb movement recognition system. As consolidated in Table II and III and summarized in Section IV-A, the features deduced from the sEMG sources that are estimated via ICA-EBM have been proven to facilitate the classifier performance significantly, when the study involved either the normal subjects or those diagnosed with knee disorders. Therefore we are led to infer that the source-separated sEMG signals collected from the hamstring (st and bf) as well as the quadriceps muscle (vm and rf) activities can help accurately label the knee movement, thereby enabling one to investigate the changes due to knee pathology. In addition to the advantages of electromyogram listed in Section IV-B, the sEMG-based assessment of lower limb movements is highly desirable as it lends itself to potential applications such as controlling exoskeleton devices to support the knee. Moreover, it has the ability to diagnose or monitor knee pathologies and to evaluate the effectiveness of therapy.

This study enabled us to comprehend the inherent limitations of an sEMG classifier. First, the conclusions drawn

from an experiment exclusively involving a specific gender cannot be straightforwardly translated to participants from the other gender. Second, as common to most studies, the clinical feasibility of this method can only be validated with a large sample size that would reduce any possible bias induced by a smaller sample. Third, notwithstanding the promising outcome in the pilot study, further research is warranted to ameliorate its classification performance to commensurate with the stringent requirements of prosthetic limb control. Being cognizant of these factors, our future objective is to apply this framework with diverse groups of individuals and also possibly with amputee subjects by incorporating activities such as stair ascent and descent. Aside from this, we intend to further explore this approach with control mechanisms of neural-controlled artificial legs for assisting lower limb amputees.

ACKNOWLEDGMENT

The authors would like to thank Shyamala Magdalene for proofreading this article and Raza Husain for insightful discussion. Furthermore, they appreciate the anonymous reviewers and the Associate Editor for their valuable comments that enabled them improve the article.

REFERENCES

[1] H. He, K. Kiguchi, and E. Horikawa, "A study on lower-limb muscle activities during daily lower-limb motions," *International Journal of Bioelectromagnetism*, vol. 9, no. 2, pp. 79–84, 2007.

[2] C. D. Joshi, U. Lahiri, and N. V. Thakor, "Classification of gait phases from lower limb EMG: Application to exoskeleton orthosis," in *IEEE Point-of-Care Healthcare Technologies (PHT)*. IEEE, 2013, pp. 228–231.

[3] J. Rafiee, M. A. Rafiee, F. Yavari, and M. P. Schoen, "Feature extraction of forearm EMG signals for prosthetics," *Expert Systems with Applications*, vol. 38, no. 4, pp. 4058–4067, 2011.

[4] R. N. Khushaba, S. Kodagoda, M. Takruri, and G. Dissanayake, "Toward improved control of prosthetic fingers using surface electromyogram (EMG) signals," *Expert Systems with Applications*, vol. 39, no. 12, pp. 10 731–10 738, 2012.

[5] R. Merletti and P. A. Parker, *Electromyography: Physiology, Engineering, and Non-Invasive Applications*. John Wiley & Sons, 2004, vol. 11.

[6] D. C. Preston and B. E. Shapiro, *Electromyography and Neuromuscular Disorders: Clinical-Electrophysiologic Correlations (Expert Consult-Online)*. Elsevier Health Sciences, 2012.

[7] G. S. Murley, K. B. Landorf, H. B. Menz, and A. R. Bird, "Effect of foot posture, foot orthoses and footwear on lower limb muscle activity during walking and running: A systematic review," *Gait & Posture*, vol. 29, no. 2, pp. 172–187, 2009.

[8] G. S. Murley, H. B. Menz, K. B. Landorf, and A. R. Bird, "Reliability of lower limb electromyography during overground walking: A comparison of maximal and sub-maximal normalisation techniques," *Journal of Biomechanics*, vol. 43, no. 4, pp. 749–756, 2010.

[9] M. O. Ericson, R. Nisell, and J. Ekholm, "Quantified electromyography of lower-limb muscles during level walking," *Scandinavian Journal of Rehabilitation Medicine*, vol. 18, no. 4, pp. 159–163, 1985.

[10] A. Rainoldi, G. Melchiorri, and I. Caruso, "A method for positioning electrodes during surface EMG recordings in lower limb muscles," *Journal of Neuroscience Methods*, vol. 134, no. 1, pp. 37–43, 2004.

[11] S. Mulroy, J. Gronley, W. Weiss, C. Newsam, and J. Perry, "Use of cluster analysis for gait pattern classification of patients in the early and late recovery phases following stroke," *Gait & Posture*, vol. 18, no. 1, pp. 114–125, 2003.

[12] H. Huang, F. Zhang, L. J. Hargrove, Z. Dou, D. R. Rogers, and K. B. Englehart, "Continuous locomotion-mode identification for prosthetic legs based on neuromuscular–mechanical fusion," *IEEE Trans. Biomed. Eng.*, vol. 58, no. 10, pp. 2867–2875, 2011.

[13] G. Bovi, M. Rabuffetti, P. Mazzoleni, and M. Ferrarin, "A multiple-task gait analysis approach: Kinematic, kinetic and EMG reference data for healthy young and adult subjects," *Gait & Posture*, vol. 33, no. 1, pp. 6–13, 2011.

[14] H. K. Choi, J. H. Jeong, S. H. Hwang, H. C. Choi, and W. H. Cho, "Feature evaluation and pattern recognition of lower limb muscle EMG during postural balance control," in *Key Engineering Materials*, vol. 326. Trans. Tech Publ., 2006, pp. 867–870.

[15] R. G. E. Clement, K. E. Bugler, and C. W. Oliver, "Bionic prosthetic hands: A review of present technology and future aspirations," *The Surgeon*, vol. 9, no. 6, pp. 336–340, 2011.

[16] H. Huang, T. A. Kuiken, and R. D. Lipschutz, "A strategy for identifying locomotion modes using surface electromyography," *IEEE Trans. Biomed. Eng.*, vol. 56, no. 1, pp. 65–73, 2009.

[17] R. M. Rangayyan, F. Oloumi, Y. Wu, and S. Cai, "Fractal analysis of knee-joint vibroarthrographic signals via power spectral analysis," *Biomedical Signal Processing and Control*, vol. 8, no. 1, pp. 23–29, 2013.

[18] J.-H. Ryu and D.-H. Kim, "Multiple gait phase recognition using boosted classifiers based on sEMG signal and classification matrix," in *Proceedings of the 8th International Conference on Ubiquitous Information Management and Communication*. ACM, 2014, p. 90.

[19] M. Janidarmian, K. Radecka, and Z. Zilic, "Automated diagnosis of knee pathology using sensory data," in *Proceedings of 4th International Conference on Wireless Mobile Communication and Healthcare (Mobihealth)*. IEEE, 2014, pp. 95–98.

[20] M. Herrera-González, G. A. Martínez-Hernández, J. L. Rodríguez-Sotelo, and Ó. F. Avilés-Sánchez, "Knee functional state classification using surface electromyographic and goniometric signals by means of artificial neural networks," *Ingeniería y Universidad*, vol. 19, no. 1, pp. 51–66, 2015.

[21] Ö. F. Ertuğrul, Y. Kaya, and R. Tekin, "A novel approach for SEMG signal classification with adaptive local binary patterns," *Medical & Biological Engineering & Computing*, vol. 54, no. 7, pp. 1137–1146, 2016.

[22] Y. Zhang, P. Xu, P. Li, K. Duan, Y. Wen, Q. Yang, T. Zhang, and D. Yao, "Noise-assisted multivariate empirical mode decomposition for multichannel EMG signals," *Biomedical Engineering Online*, vol. 16, no. 1, p. 107, 2017.

[23] G. R. Naik, S. Arjunan, and D. Kumar, "Applications of ICA and fractal dimension in sEMG signal processing for subtle movement analysis: A review," *Australasian Physical & Engineering Sciences in Medicine*, vol. 34, no. 2, pp. 179–193, 2011.

[24] G. R. Naik and D. K. Kumar, "Estimation of independent and dependent components of non-invasive EMG using fast ICA: Validation in recognising complex gestures," *Computer Methods in Biomechanics and Biomedical Engineering*, vol. 14, no. 12, pp. 1105–1111, 2011.

[25] G. R. Naik and D. K. Kumar, "Identification of hand and finger movements using multi run ICA of surface electromyogram," *Journal of Medical Systems*, vol. 36, no. 2, pp. 841–851, 2012.

[26] X.-L. Li and T. Adalı, "A novel entropy estimator and its application to ICA," in *IEEE International Workshop on Machine Learning for Signal Processing*. IEEE, 2009, pp. 1–6.

[27] X.-L. Li and T. Adalı, "Blind spatiotemporal separation of second and/or higher-order correlated sources by entropy rate minimization," in *IEEE International Conference on Acoustics, Speech and Signal Processing*. IEEE, 2010, pp. 1934–1937.

[28] X.-L. Li and T. Adalı, "Independent component analysis by entropy bound minimization," *IEEE Trans. Signal Process.*, vol. 58, no. 10, pp. 5151–5164, 2010.

[29] S. E. Selvan, S. T. George, and R. Balakrishnan, "Range-based ICA using a nonsmooth quasi-Newton optimizer for electroencephalographic source localization in focal epilepsy," *Neural Computation*, vol. 27, no. 3, pp. 628–671, 2015.

[30] I. W. Hunter, R. E. Kearney, and L. A. Jones, "Estimation of the conduction velocity of muscle action potentials using phase and impulse response function techniques," *Medical and Biological Engineering and Computing*, vol. 25, no. 2, pp. 121–126, 1987.

[31] M. Bilodeau, M. Cincera, A. B. Arsenault, and D. Gravel, "Normality and stationarity of EMG signals of elbow flexor muscles during ramp and step isometric contractions," *Journal of Electromyography and Kinesiology*, vol. 7, no. 2, pp. 87–96, 1997.

[32] K. Nazarpour, A. H. Al-Timemy, G. Bugmann, and A. Jackson, "A note on the probability distribution function of the surface electromyogram signal," *Brain Research Bulletin*, vol. 90, pp. 88–91, 2013.

[33] M. Anderson, X.-L. Li, P. Rodriguez, and T. Adalı, "An effective decoupling method for matrix optimization and its application to the ICA problem," in *Proceedings of International Conference on Acoustics, Speech, and Signal Processing*. IEEE, 2012, pp. 1885–1888.

[34] A. Hyvärinen, "Fast and robust fixed-point algorithms for independent component analysis," *IEEE Trans. Neural Netw.*, vol. 10, no. 3, pp. 626–634, 1999.
[35] T. Higuchi, "Approach to an irregular time series on the basis of the fractal theory," *Physica D: Nonlinear Phenomena*, vol. 31, no. 2, pp. 277–283, 1988.
[36] A. Golestani, M. R. J. Motlagh, K. Ahmadian, A. H. Omidvarnia, and N. Mozayani, "A new criterion to distinguish stochastic and deterministic time series with the poincaré section and fractal dimension," *Chaos: An Interdisciplinary Journal of Nonlinear Science*, vol. 19, no. 1, p. 013137, 2009.
[37] B. Hosseinifard, M. H. Moradi, and R. Rostami, "Classifying depression patients and normal subjects using machine learning techniques and nonlinear features from EEG signal," *Computer Methods and Programs in Biomedicine*, vol. 109, no. 3, pp. 339–345, 2013.
[38] R. Esteller, G. Vachtsevanos, J. Echauz, and B. Litt, "A comparison of waveform fractal dimension algorithms," *IEEE Transactions on Circuits and Systems I: Fundamental Theory and Applications*, vol. 48, no. 2, pp. 177–183, 2001.
[39] M. Zhu and A. Ghodsi, "Automatic dimensionality selection from the scree plot via the use of profile likelihood," *Computational Statistics & Data Analysis*, vol. 51, no. 2, pp. 918–930, 2006.
[40] O. F. A. Sanchez, J. L. R. Sotelo, M. H. Gonzales, and G. A. M. Hernandez, "EMG dataset in lower limb data set - UCI machine learning repository," 2013.
[41] L. Hargrove, K. Englehart, and B. Hudgins, "A training strategy to reduce classification degradation due to electrode displacements in pattern recognition based myoelectric control," *Biomedical Signal Processing and Control*, vol. 3, no. 2, pp. 175–180, 2008.
[42] A. D. C. Chan and G. C. Green, "Myoelectric control development toolbox," in *Proceedings of 30th Conference of the Canadian Medical & Biological Engineering Society*, vol. 1, 2007, pp. M0100–1.
[43] G. R. Naik and H. T. Nguyen, "Nonnegative matrix factorization for the identification of EMG finger movements: Evaluation using matrix analysis," *IEEE Journal of Biomedical and Health Informatics*, vol. 19, no. 2, pp. 478–485, 2015.
[44] S. P. Arjunan and D. K. Kumar, "Decoding subtle forearm flexions using fractal features of surface electromyogram from single and multiple sensors," *Journal of Neuroengineering and Rehabilitation*, vol. 7, no. 1, pp. 1–10, 2010.
[45] A. L. Goldberger, L. A. N. Amaral, J. M. Hausdorff, P. C. Ivanov, C.-K. Peng, and H. E. Stanley, "Fractal dynamics in physiology: Alterations with disease and aging," *Proceedings of the National Academy of Sciences*, vol. 99, no. suppl 1, pp. 2466–2472, 2002.
[46] A. Y. Meigal, S. M. Rissanen, M. P. Tarvainen, O. Airaksinen, M. Kankaanpää, and P. A. Karjalainen, "Non-linear EMG parameters for differential and early diagnostics of parkinson's disease," *Frontiers in Neurology*, vol. 4, 2013.
[47] M. K. Zebis, J. Skotte, C. H. Andersen, P. Mortensen, H. H. Petersen, T. C. Viskær, T. L. Jensen, J. Bencke, and L. L. Andersen, "Kettlebell swing targets semitendinosus and supine leg curl targets biceps femoris: An EMG study with rehabilitation implications," *British Journal of Sports Medicine*, vol. 47, pp. 1192–1198, 2012.
[48] Y. Makihara, A. Nishino, T. Fukubayashi, and A. Kanamori, "Decrease of knee flexion torque in patients with ACL reconstruction: Combined analysis of the architecture and function of the knee flexor muscles," *Knee Surgery, Sports Traumatology, Arthroscopy*, vol. 14, no. 4, pp. 310–317, 2006.
[49] T. W. Kernozek, M. R. Torry, and M. Iwasaki, "Gender differences in lower extremity landing mechanics caused by neuromuscular fatigue," *The American Journal of Sports Medicine*, vol. 36, no. 3, pp. 554–565, 2008.
[50] S. C. Landry, K. A. McKean, C. L. Hubley-Kozey, W. D. Stanish, and K. J. Deluzio, "Neuromuscular and lower limb biomechanical differences exist between male and female elite adolescent soccer players during an unanticipated side-cut maneuver," *The American Journal of Sports Medicine*, vol. 35, no. 11, pp. 1888–1900, 2007.

Ganesh R. Naik (M'08–SM'15) received the Ph.D. degree in biomedical signal processing from RMIT University, Melbourne, Australia, in 2009. He was a Chancellor's Post-Doctoral Research Fellow, University of Technology Sydney. Since July 2017 he has been a Post-Doctoral Research Fellow at MARCS Institute, Western Sydney University. He has edited 10 books, authored more than 100 papers in peer reviewed journals, conferences, and book chapters. Dr. Naik serves as an Associate Editor for IEEE Access, Frontiers in Neurorobotics, and two Springer journals. In 2010, he was awarded an ISSI overseas fellowship from Skilled Institute Victoria, Australia.

S. Easter Selvan received the Ph.D. degree in multispectral satellite image analysis from Université de la Méditerranée, Marseille, France, in 2007. He was a Post-Doctoral Fellow at Consiglio Nazionale delle Ricerche, Naples, Italy, from 2008 to 2010, at Université catholique de Louvain, Louvain-la-Neuve, Belgium, from 2010 to 2014, and at Université Joseph Fourier, Grenoble, France, from 2014 to 2015. He has been an Associate Research Scientist at Kessler Foundation, West Orange, NJ, U.S.A., since 2015. His research focus encompasses statistical signal processing, blind source separation, medical imaging, optimization on matrix manifolds, machine learning, bio-signal analysis, and rehabilitation engineering.

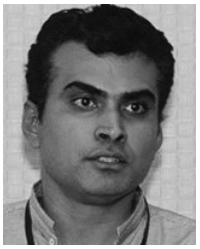

Sridhar P. Arjunan (M'09–SM'15) received the Ph.D. degree in biomedical signal processing from RMIT University, Melbourne, Australia, in 2009. He is a Post-Doctoral Research Fellow with the Biosignals Lab at RMIT University, and associated with SRM University, Chennai, India. He has over 100 research publications and has co-authored three books. Dr. Arjunan is a recipient of the Australia-India Early Career Fellowship, RMIT SECE Research Scholarship, German State Research Scholarship, and CASS Australian Early Career Researcher Grant. His major research interests include biomedical signal processing, fractal theory, multi-spectral analysis, diagnostic devices, and human-computer interface applications.

Amit Acharyya (M'11) received the Ph.D. degree from the School of Electronics and Computer Science, University of Southampton, Southampton, U.K., in 2011. He is currently an Associate Professor with the Indian Institute of Technology (IIT) Hyderabad, India. His current research interests include signal processing algorithms, VLSI architectures, low power design techniques, computer arithmetic, numerical analysis, linear algebra, bioinformatics, and the electronic aspects of pervasive computing.

Dinesh Kumar (M'95) received the Ph.D. degree from IIT, Delhi, India. He is a Professor with the Biomedical Engineering Department, RMIT University, Melbourne, Australia, and a Visiting Professor at IIT, Gandhinagar, India and University Federal, Brazil. He has extensive experience in technology translation, and is managing two technology start-up ventures. He has authored a book entitled, "Research Methods for Successful PhD". Dr. Kumar is a Member of the Therapeutic Goods Administration Advisory Panel, Ministry of Health for Medical Devices, and a Fellow, IIT, Gandhinagar, India. He is leading a research team whose interests include bio-signal processing, medical image analysis, and machine learning.

Arvind Ramanujam received the M.S. degree in biomedical engineering from Drexel University, Philadelphia, U.S.A. in 2006. In 2005-06, he performed research at the Baylor College of Medicine (respiratory biomechanics) as an Intern and later at the Steadman Hawkins Sports Medicine Foundation (3D inverse dynamics in sports biomechanics) as a Scientist. He is now employed with Kessler Foundation as a Senior Engineer in the HPE Laboratory conducting rehabilitation and quality of life research for patients with stroke and spinal cord injury. His research interests include human performance analysis, musculoskeletal modeling, robotics, rehabilitation/sports biomechanics, and biomedical signal processing.

Hung T. Nguyen (SM'99) received the Ph.D. degree in 1980 from the University of Newcastle, Australia. He is the Pro Vice-Chancellor for Faculty of Science, Engineering & Technology at Swinburne University of Technology, Melbourne, Australia. He is a Senior Member of the Institute of Electrical and Electronic Engineers, and a Fellow of the Institution of Engineers, Australia, the British Computer Society as well as the Australian Computer Society. His research interests include biomedical engineering, artificial intelligence, neurosciences, and advanced control. He has developed medical devices for diabetes, disability, fatigue, and cardiovascular diseases.